Materials Today Communications 22 (2020) 100792

Contents lists available at ScienceDirect

Materials Today Communications

journal homepage: www.elsevier.com/locate/mtcomm

Not all scans are equal: X-ray tomography image quality evaluation

A. du Plessis[a,b,*], M. Tshibalanganda[a], S.G. le Roux[a,1]

[a] CT Scanner Facility, Stellenbosch University, Stellenbosch, 7602, South Africa
[b] Physics Department, Stellenbosch University, Stellenbosch, 7602, South Africa

ARTICLE INFO

Keywords:
X-ray tomography
microCT
Materials science
Quality control
Image quality

ABSTRACT

X-ray microtomography is widely used in materials science and engineering applications for imaging and analysis of material structure and morphology. For this purpose, and especially in the case of routine analysis tasks for industrial materials applications, confidence in obtained measurement results are crucial. Despite great progress in this field over the last 10 years, with many high-quality commercial systems now available, the lack of a simple and widely-used image quality metric that can capture all important aspects of the quality of a microCT scan, continues to hinder wider acceptance of the technology. Various errors can occur during the microCT scan process, which can potentially mask the presence of pores, or affect the volumetric measurements of interest. In this work we demonstrate a simplified image quality metric which can easily be implemented. We show how this new image quality metric is sensitive to all typical microCT scan errors and artifacts, which makes it a valuable tool for defining a required minimum image quality for an analysis. The object used is a 10 mm cube of titanium alloy (Ti6Al4V) produced by laser powder bed fusion additive manufacturing. This type of coupon sample is useful for analysis of the additive manufacturing process, but it is critical that small pores are seen with good contrast. Identical porosity analysis workflows are applied to scans with different image qualities, which demonstrates the importance of image quality for reproducible analyses of this sample type. The results have implications in defining quality values for all forms of materials analysis using the technique. This work can further lead the way to incorporating microCT into future fully automated and standardized analysis workflows for quality control, when image quality meets a specified minimum criterion.

1. Introduction

X-ray micro computed tomography (also known as X-ray microtomography or micro-CT) is a non-destructive materials imaging and analysis technique growing in popularity in materials science and engineering applications. This growth can be attributed to its many advantages – particularly the ability to visualize internal structures of materials in three dimensions and without the need for destructive sectioning. Besides visualization, numerous quantitative analyses are possible, the most well-known being porosity quantification. The use of the technique in materials science applications was reviewed in [1], which highlights the quantitative capabilities for three-dimensional materials characterization. All kinds of engineering and other materials benefit from non-destructive 3D analysis, as shown in reviews of the technique applied to geomaterials [2], asphalt and concrete materials [3], additively manufactured materials [4], composites [5], biological samples [6], herpetology [7], natural structures as basis for engineering design i.e. biomimicry [8], amongst others. Besides research applications, the technique is also very useful for non-destructive testing and process improvement in industrial applications – various industrial applications are demonstrated in [9,10]. As shown in these papers, the technique is becoming an accepted non-destructive test method for industrial inspection of injection moulded parts, cast metal parts and is especially useful for inspection of high-value parts such as those in aerospace and energy production industries. In addition to inspection, the dimensional measurement capability of the technique allows it to be used as a metrology tool, as discussed in detail in [11,12]. For metrology applications, dimensional calibration is important and various test artifacts have been proposed and demonstrated for this purpose [13–15].

Despite all the application possibilities and the proven utility of the technique, and despite the successful dimensional calibration efforts, the method is still plagued by some reliability issues. This is due to the large variety of instrument types available (ranging from small benchtop models to large bunker systems and even synchrotron imaging beamlines), differences in hardware and software used for image

* Corresponding author at: CT Scanner Facility, Stellenbosch University, Stellenbosch, 7602, South Africa.
E-mail address: anton2@sun.ac.za (A. du Plessis).
[1] Now at Bruker microCT, Kontich 2550, Belgium

https://doi.org/10.1016/j.mtcomm.2019.100792
Received 15 September 2019; Received in revised form 20 November 2019; Accepted 21 November 2019
Available online 22 November 2019
2352-4928/

analysis and differences in the skill-sets and experience levels of the scientists or operators doing the scanning (optimization of parameters, etc.) and subsequent image interpretation or analysis. It can be well understood that different systems are suited to different tasks, with image quality differences to be expected. The quality of obtained images is therefore critical to ensure positive identification of flaws and also critical to accurate quantification in images (e.g. porosity %). Post-scan image analysis is discussed in detail in [16], also mentioning image quality evaluation and good image quality as a prerequisite for further image analysis.

The drawback to high image quality is usually cost, as more expensive systems and longer scan times are required. However, to date there is not a wide understanding of this challenge. Especially new users of the technology aim to minimize scan times, which can significantly reduce image quality. For improved uptake of the technology, and to improve the confidence in the obtained results, an accepted and reliable image quality metric would be very helpful, which is widely applicable and easy to apply to any micro-CT data set. The grey values obtained in CT images (typically 8-bit or 16-bit type) are such that different materials have different distinct grey value ranges. These ranges vary in their extent and their separation from each other in the grey value histogram, making it easier or more difficult to clearly distinguish the materials from each other (contrast). In addition, inherent noise exists in the background and the material, due to detector and other noise inherent in the data acquisition process. In addition to material contrast and noise, the image sharpness (which is mainly due to the inherent resolution of the system) is highly important. All these parameters were recently investigated separately in a comprehensive study of image quality improvement for scanning of fossils embedded in rocks [17] as a case study to illustrate optimized scan parameters for this particular sample type. A similar study was recently reported for porosity analysis of carbonate rocks in [18], as well as for fast iterative reconstruction and optimization of image quality for porous rocks in [19]. More generally the effect of scan parameters on CT images was also reported in [20], and image quality and reproducibility were studied in scans for geoscience applications in [21].

Image quality evaluation in CT images is an ongoing issue in the field, as there has thus far not been a universally relevant and simple method to quantify this important parameter. An existing ASTM standard exists for measuring image quality in CT scans, but this is limited to a single slice image of a cylindrical object scanned exactly vertically, which was developed for fan-beam CT in particular [22]. This standard is not suited to cone-beam CT systems (which are more widely used) and the afore-mentioned measurement is not a global image quality metric for the entire 3D volume, it represents the quality in a single slice only. Quality measurement of full cone-beam micro-CT images have been investigated in the context of dimensional measurements in [23] and a proposed metric incorporating all important factors above was proposed in [24], based on the grey-value histogram representing the grey-value data in the entire volume. This latter method is easy to implement and therefore is very promising as a widely used metric for image quality incorporating contrast, noise and sharpness of images in one measurement. It was however not demonstrated or tested over different scan parameters yet, and uses the histogram for measurements. This can be challenging to implement objectively, as the distributions are not always Gaussian or symmetrical.

In addition to image quality variations which exist between different scans, which can be controlled to some extent by good choices of scan parameters and good choice of system for the required sample, various other unexpected scanning errors can occur. These include double-edges, streak-artifacts, ring artifacts, beam hardening, amongst others. All these also degrade image quality, making it sometimes impossible to properly evaluate the obtained data. Such CT errors have been investigated and demonstrated in various works, see for example [6,25–27].

In this paper we make use of an additively manufactured coupon sample (10 mm cube of Ti6Al4V alloy) which has been well characterized in prior work. It was the subject of a previous round robin test [28], where 10 different participants using different micro-CT instruments and experience levels all scanned the same object using prescribed parameters and identified the main pore distribution correctly, ie. small spherical pores all under one surface primarily, with few other pores in the sample. Despite the positive identification of the pore distribution, the different scans of the same object had inherently different image qualities, making quantitative evaluation and comparison difficult. This highlighted the need for a globally relevant image quality metric, as well as the need for good image quality for quantitative measurements from microCT scans.

In this present work we use the same cube and quantify image quality across a series of scans with varying parameters and including various artifacts induced intentionally. In this way the utility of the image quality metric is demonstrated, various typical artifacts are demonstrated, and their effects on the image quality metric also quantified. Besides the modified image quality measure for the entire cube similar to the previously suggested metric, we use in addition a modified version of the same method applied to the material surface region only (5 voxels on either side), which provides an improved measure of sharpness or blur in the image. This sharpness is critical for small pore detection and is not captured in the simple first-level image quality metric making use of the entire cube and all air around it.

Quantification of porosity in the 10 mm cube of Ti6Al4V was done according to a prescribed workflow [29], and this is further used to evaluate the reliability of the workflow, with different image qualities. This work aims to support standardization efforts towards improving the reliability and reproducibility of microCT as applied to materials science and engineering projects generally. It also brings home the message that “not all scans are equal” – a common misconception among new users to this technology. In addition, the work serves as demonstration of the effect of each typical CT artifact, which will assist new users of this technology.

2. Methods

X-ray tomography was performed at the Stellenbosch CT facility using two different systems – microCT and nanoCT systems [30]. The microCT refers to a typical laboratory system with reflection-type X-ray source with minimum focal spot size approximately 5 µm (model GE Vtomex L240). NanoCT refers to a system with transmission-type X-ray source with best spot size below 1 µm, allowing (in principle) voxel sizes to 0.5 µm (model GE Nanotom S). A single microCT data set was used as good “reference” example, and a series of scans were conducted on the nanoCT system. The two systems have different types of sources and detectors, the latter mainly affecting the contrast and background noise levels. A single cube was used which originated from two previous round robin studies [28,31], and which was produced by laser powder bed fusion [32] using a commercial system using Ti6Al4V powder. The selected 10 mm cube contains small rounded pores subsurface of the top surface of the cube (relative to its build orientation), making a good qualitative test for image quality due to the small size and specific location of these pores. This is a particularly challenging quantitative analysis due to the small size of the pores (largest pore 0.2 mm) and small mean porosity value (~0.02 %).

The image quality metric proposed in [24] is used in this work in a modified format, it is defined as follows:

$$Q = \frac{|\mu_2 - \mu_1|}{\sqrt{\sigma_1^2 + \sigma_2^2}}$$

Where μ is the mean grey value and σ is the standard deviation of the histogram distribution for material (2) and air (1) respectively. In the work in [24], the values were obtained from the histogram distribution with potentially overlapped peaks for air and material. In this work we

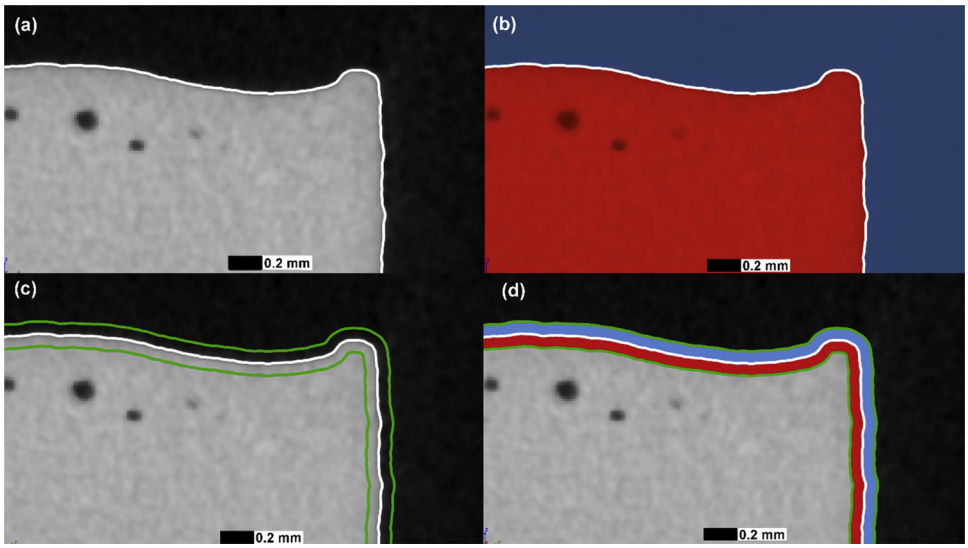

Fig. 1. Close-up of corner of cube in microCT slice image showing (a) surface determination in white line; (b) segmentation of air (blue) and material (red) allowing quality value Q1 to be calculated; (c) near-surface region of interest of 5 voxels on either side of surface (green); (d) near-surface segmentation of air (blue) and material (red) allowing quality value Q2 to be calculated (For interpretation of the references to colour in this figure legend, the reader is referred to the web version of this article).

segment the data first, to obtain separate histograms for material and for air, simplifying the quantitative analysis. In addition, the direct measurement of mean and standard deviation from the software package used eliminates an additional step of processing (obtaining the values from a histogram output). In this work, the grey value analysis tool in VGSTUDIO MAX was used after segmentation to provide effectively analysis of each phase (material and air) separately.

In addition to this modification, we propose an additional step to create two different quality factors based on two segmentations. In the first step, the values are obtained from the entire cube material data and all air data outside the cube (separately), using the surface determination function to differentiate these from each other – this is illustrated in Fig. 1(a) and (b). In the second step, the same analysis is made using values obtained from the region near the edge of the cube only – 5 voxels on either side of the surface of the cube which is illustrated in Fig. 1 (c) and (d). This latter step is implemented using the "create ROI from surface" function and applying a thickness equivalent to 10 voxels. The first image quality metric is sensitive mainly to contrast and noise, providing a good "first-level" quality measure, which we call Q1. The second is more sensitive to blur or loss of sharpness which occurs more at edges of the material and we call this Q2.

A video is included as supplementary material, to demonstrate how the above values are found from the CT data set. In a hypothetical "ideal" case with material and air having grey value distributions with infinitely sharp and narrow peaks, the value of the denominator in the Q-value calculation strives to zero and therefore the Q value strives to infinity. This means there is theoretically no upper limit on the quality value. A realistic "ideal case" was created as a test in VGSTUDIO MAX using a 10 mm cube defined and created as an artificial voxel data set with 10 µm voxel size, in the same scan volume as a typical cube scan. The air and material values were artificially smoothed and normalized to 0 and 65,535 and the edge sharpness was only limited by the 10 µm voxel size and rotation of the voxel grid with respect to the edges of the cube, creating some region of partial volume effect. The obtained "ideal" values for this artificial dataset was found to be Q1 = 68 and Q2 = 13, which gives a good indication of a maximum image quality possible.

The experimental campaign is divided into two parts: (a) demonstrating the image quality Q1 and Q2 value variation with different types of scans and incorporating different typical image artifacts, and (b) applying image analysis on a series of data sets of the same sample, with varying image quality – to demonstrate the need for high image quality for reliable image analysis. The series of scans with induced image quality differences are summarized in Table 1.

3. Image quality results

3.1. Machine change

A change of machine from microCT to nanoCT in this case resulted in a quality Q1 value reduction from 8.6 to 4.5, with this reduction clear in the images in Fig. 2. Both scans are optimized and total 1 h scan time. The quality Q2 values are 3.7 and 3.3 for microCT and nanoCT respectively. The larger difference in Q1 values can be attributed to the microCT detector having a 16-bit data depth while the nanoCT detector has only 12-bit data depth; this difference ensures greater contrast for the microCT system which is better captured by the Q1 value. Both images are sharp making the Q2 values more similar despite the obvious increased noise in the nanoCT image to the right.

3.2. Scan time

Scans with increased scan time (increased image averaging and number of projection angles) is shown in Fig. 3 to improve the image quality. The Q1 image quality value (circles) continues to improve with increasing scan time due to reduced noise but this increase starts to reach a plateau level. In practical terms, longer scans effectively limit the sample throughput and increase the cost to the user, therefore a compromise is usually sought after. The Q2 value increases strongly up to approximately 1 h, thereafter reaching a plateau level with some variation observed (dip in value at 2 h). This reduced value at 2 h can be due to some slight change in the system stability, X-ray flux or detector response, as this scan was conducted on a different day. As seen in Fig. 4 in representative slice images, this particular system seems to require at least 2 h to obtain reasonable image quality for this sample type, which translates to quality values Q1 > 6, and Q2 > 3.

3.3. Voltage change

In this experiment, three voltages were selected covering the range of most laboratory microCT instruments: 50, 100 and 150 kV. Beam filters were used and current adjusted to ensure the same detector counts, for direct comparison – in this case no filters at 50 kV or 100 kV (lower current at higher voltage) and 0.5 mm copper filter at 150 kV. In this series, as seen in Fig. 5, the image quality improves with increasing voltage – with less brightness variations are evident at higher voltage. This translates to quality Q1 values of 2.9, 3.5 and 5.4 respectively in the series shown. The pores near the top surface are not well distinguished as seen in the images. The best result is at highest voltage as

Table 1
Image quality variation test summary – total of 23 data sets.

Test name	Details
Change machine	MicroCT vs NanoCT 1 hr optimized each
Vary scan time	3 min; 20 min; 45 min; 2 hrs; 3 hrs; 4 hrs
Vary voltage	50 kV; 100 kV; 150 kV
Induce streak artifact	One scan with dense metal alongside cube
Sample mounting error 1	Cube mounted square – cone beam artifacts on flat edges
Sample mounting error 2	Cube mounted unstable
Dead pixels on detector	Dead pixels of detector causing bright rings
Double edges	Reconstruction "centre of rotation" error causing increasing double-edge in images, values of 5, 10, 20 pixels offset from ideal
Beam hardening correction	Increasing beam hardening correction values to correct cupping effect – 5 variations
Rotation rings	Scans with and without detector shift

expected for this sample type, as metals are typically scanned using higher voltage for better penetration of X-rays through the sample. The Q1 value clearly identifies the expected trend that lower voltage results in a large variation of brightness values resulting in a lower Q1 value. For Q2 which gives an indication of the sharpness in the images, the values are 1.4, 1.1 and 2.1, which are all very poor compared to the reference nanoCT scan (Q2 = 3.3).

3.4. Streak artifact

The use of a dense metal object placed alongside the cube induced streak artifacts in the image. This makes it challenging to segment the cube from the rest of the image and makes the image quality measurement impossible. A slice image is shown in Fig. 6 where the streaks are visible inside the cube at the bottom of the image, due to the dense material outside the cube – in this case gold was used. The cube is scanned at an angle and in this case the image is kept in the same orientation as in the scan, to demonstrate the horizontal nature of the streaks – in the direction of the X-ray beam perpendicular to the rotation axis.

3.5. Sample mounting errors

Two sample mounting errors are demonstrated here. The first is to load the cube perfectly square relative to the X-ray beam direction, this causes cone-beam artifacts along the flat edges of the cube which are almost always parallel to the beam during sample rotation (in this case top and bottom of cube) as seen in Fig. 7. In this case the image quality Q1 value is 3.9 (compared to ideal case of 4.5) – only a slight reduction. The Q2 value here is 1.8 compared to 3.3 of the ideal case, indicating the loss in sharpness especially on some of the edges. The pores of interest in this case lie in the region which seems darker due to the cone beam artifact. This can affect the image analysis process and can potentially mask pores.

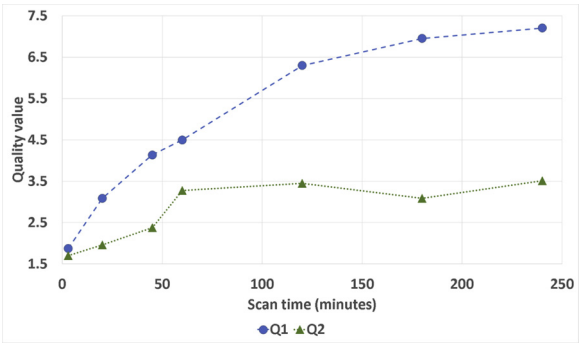

Fig. 3. Image quality Q1 and Q2 increase with increasing scan time. Both Q1 and Q2 increase with time. The Q2 value (sharpness) improves up to 1 h, then saturates. Slight decrease in Q2 value seen at 3 hs.

Another important sample mounting issue is proper fixture of the sample to the rotation hardware. A loose mounting of the cube causes the sample to move slightly (e.g. due to vibration) during scanning which effectively blurs the image. The resulting image in Fig. 8 shows no pores where they are expected and the edges of the sample are also blurred. The Q1 image quality value here is 3.6 (reference 4.5), and Q2 value is 1.9 (reference 3.3).

3.6. Dead pixel rings

An image artifact that occurs due to detector pixels that are not

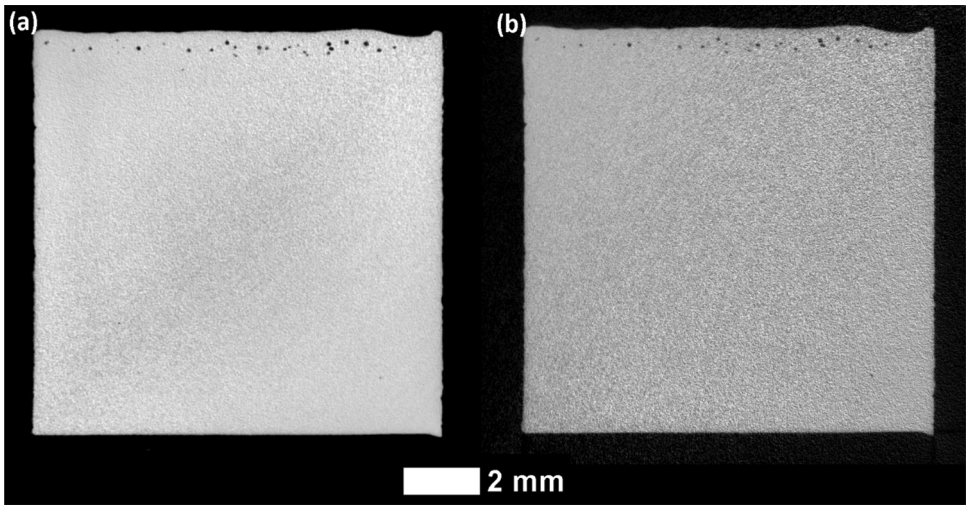

Fig. 2. Representative CT slice images for optimized scans using (a) microCT and (b) nanoCT.

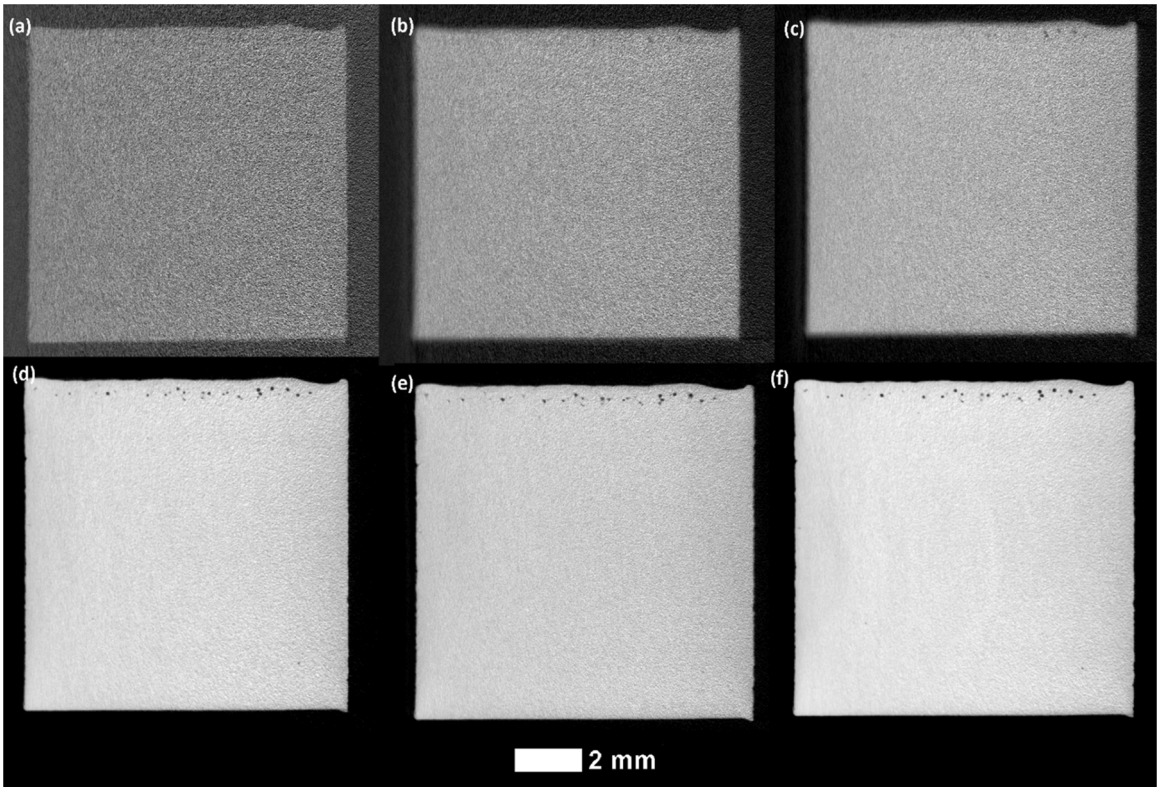

Fig. 4. Representative CT slice images with increasing scan time: (a) 3 min, (b) 20 min, (c) 45 min, (d) 2 h, (e) 3 hs, (f) 4 hs.

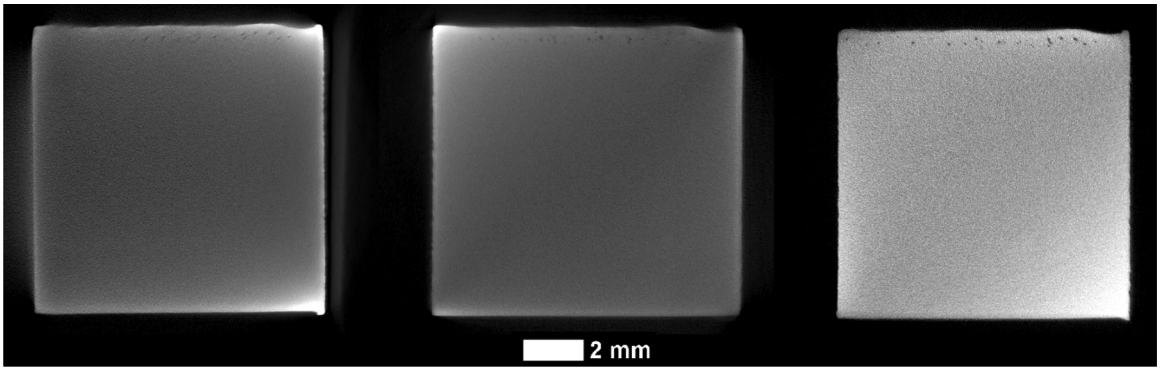

Fig. 5. Slice images showing that voltage increase improves the image quality for the titanium alloy (Ti6Al4V) cube.

responding (i.e. dead pixels) is that rings occur in the reconstructed data – this affects the contrast of the material and might interfere with segmentation. An extreme case is shown in Fig. 9, and the effective image quality Q1 value here is 0.9, showing this is well covered in the quality metric. The value of Q2 is 3.1 here (reference 3.3) showing that in this case there is no loss in sharpness – the loss is in contrast primarily.

3.7. Double edges

During reconstruction, the rotation centre is calculated for optimized reconstruction resulting in sharp images. When this rotation centre is offset slightly from the ideal value, it causes a blur or in extreme cases a “double edge”. This is demonstrated in Fig. 10 with zero offset and offset values intentionally used with values of 5, 10 and 20 pixels offset from the rotation axis. Clearly, the ability to distinguish the pores near the top surface is reduced considerably as the offset is increased. The image quality value changes are graphically illustrated in Fig. 11, with the Q2 value being very useful to highlight the loss in sharpness.

3.8. Beam hardening correction

Beam hardening correction is often employed in reconstruction software to limit the cupping artifacts associated with low energy X-rays being absorbed more strongly than high energy X-rays. The influence of this process on the resulting CT slice images is shown in Fig. 12. An increase in beam hardening correction factor tends to reduce the difference in brightness in different parts of the cube as seen in Fig. 13 (a)–(c). Ideal quality (even grey value across the cube) is shown in image (d) whereas image (e) is over-compensated. Image quality values are shown in Fig. 13 for this series, where the correction factor values range from 0 to 10 and this range is system-specific. The image quality Q1 value shows a constant decline in value with beam hardening correction, which can be attributed to an increased noise induced in the process. The value Q2 captures the sharpness of the image, and the even distribution of grey values when corrected optimally in the edge region. This shows a peak Q2 value of 3.3 at the value of 9.0 which

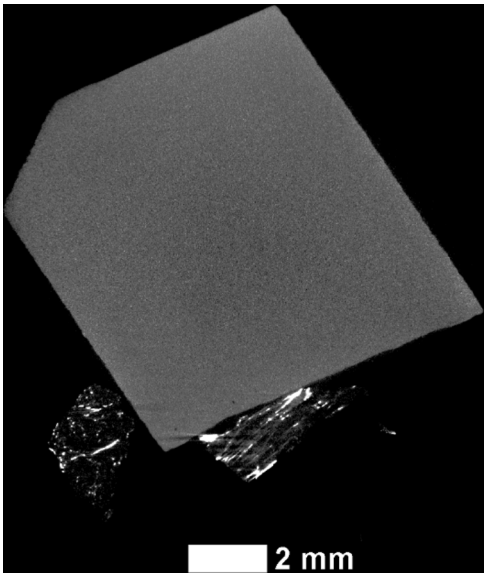

Fig. 6. Streak artifact due to denser metal alongside titanium cube – bright and dark streaks horizontally across the image make it impossible to calculate image quality values.

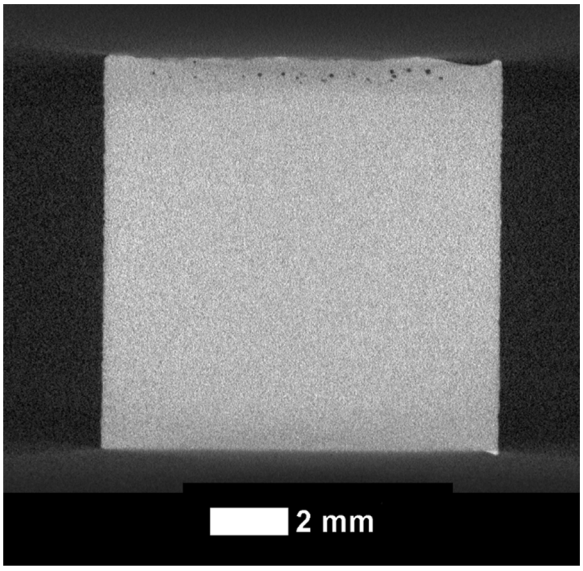

Fig. 7. Cone beam artifact along edges of cube, which can mask pores and reduces the image quality.

is the value used in practice most often for scans of metals in this system. The optimal value and then reduction of the Q2 value for higher beam hardening correction can be attributed to the over-correction which is done such that different parts of the image have different grey values, causing the value to reduce – see Fig. 12 (e).

3.9. Rotation rings

An artifact that is often found in CT images when viewed from the top (in direction of rotation axis) is the presence of circular rings around the rotation axis. This is shown in Fig. 14(a) where the dark area in the middle and sometimes in the noise of the rings themselves can be mistaken for pore spaces. This artifact can be corrected by activating a detector-shift, which is demonstrated in Fig. 14(b) where no rings are present. This detector-shift moves the detector between image acquisitions, effectively removing ring artifacts. The Q1 and Q2 values are both very similar and are therefore not sensitive to this artifact type

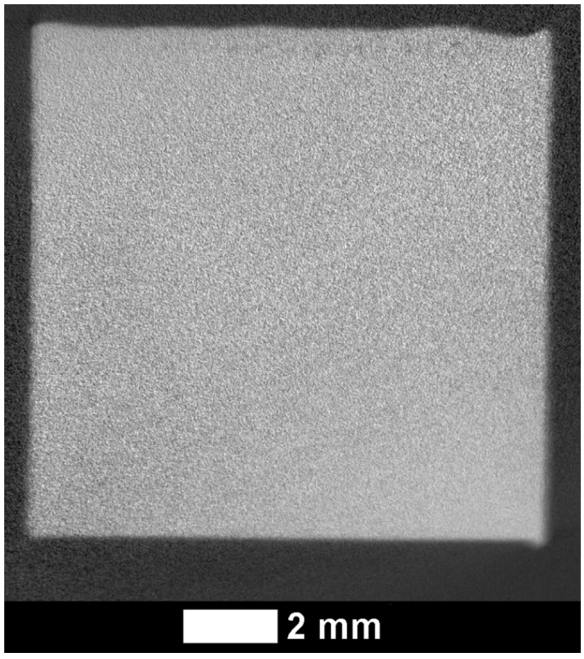

Fig. 8. Sample mounting unstable – causes serious loss of image quality.

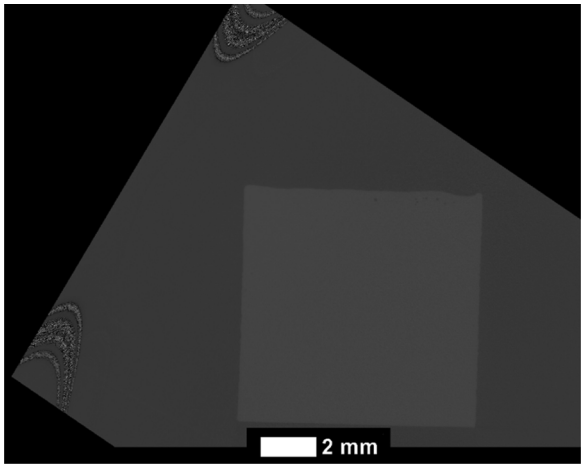

Fig. 9. Dead pixel rings reducing contrast and image quality Q1 to 0.9 in this case.

unless it interferes with the edge or makes more intense rings. In this case the Q1 and Q2 values are 4.6 and 3.1 respectively for the ring-artifact scan in Fig. 14(a), and 4.5 and 3.3 for the ideal reference in Fig. 14(b).

4. Analysis results

Analysis was performed according to the “custom defect mask” method described before. This method makes use of the iso-50 threshold as a starting point, for a local optimization of the best location of the interface between material and air. This local optimization process includes sub-voxel interpolation and improves the segmentation compared to manual image morphological segmentation and voxel binarization, removing much potential human bias. The initial choice of threshold for starting point depends on human selection based on visual inspection of images and the histogram, but this process is eased by the removal of all exterior air and surface voxels on the edge of the cube, improving the contrast and the histogram clarity.

Shown in Fig. 15 is the result of this process applied to scans of

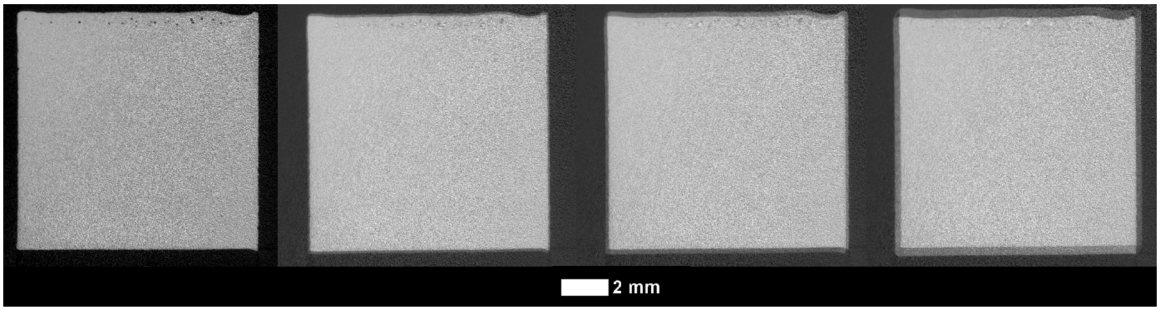

Fig. 10. Rotation offset values can cause double edges, blurring the pores and reducing the image quality.

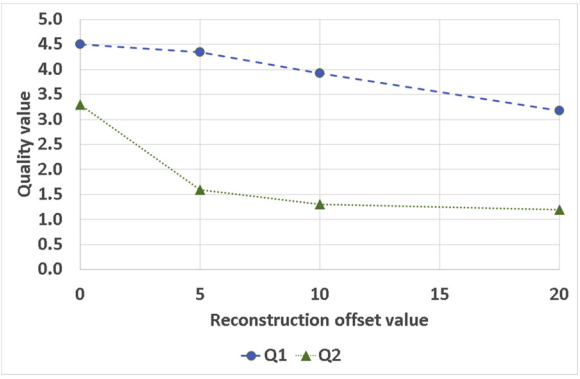

Fig. 11. Loss in image quality from reconstruction offset increase captured by both Q1 and Q2 image quality values.

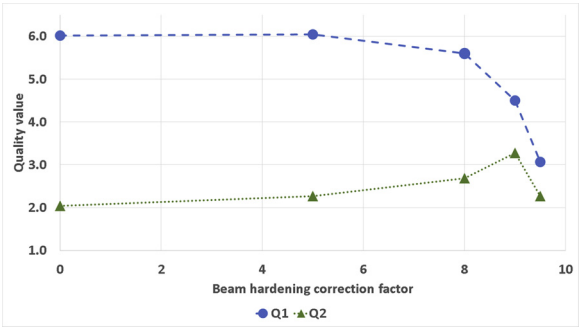

Fig. 13. Image quality Q1 and Q2 as a function of beam hardening correction factor – best result is found at correction factor of 9, captured by Q2 value.

varying scan time (and hence image quality). For each scan the segmentation was repeated by the same operator 6 times, and porosity (%) results and their standard deviations are shown. This indicates that for higher quality scans (at longer scan times), the results are similar and scans below 1 h cause errors in quantitative analysis. Mostly at short scan times, the sharpness is lower as indicated already in Fig. 3 in the previous section. This lower sharpness has the effect of reducing the detail visible and hence lower values of porosity are reported.

With longer scans there is also some variation as can be expected

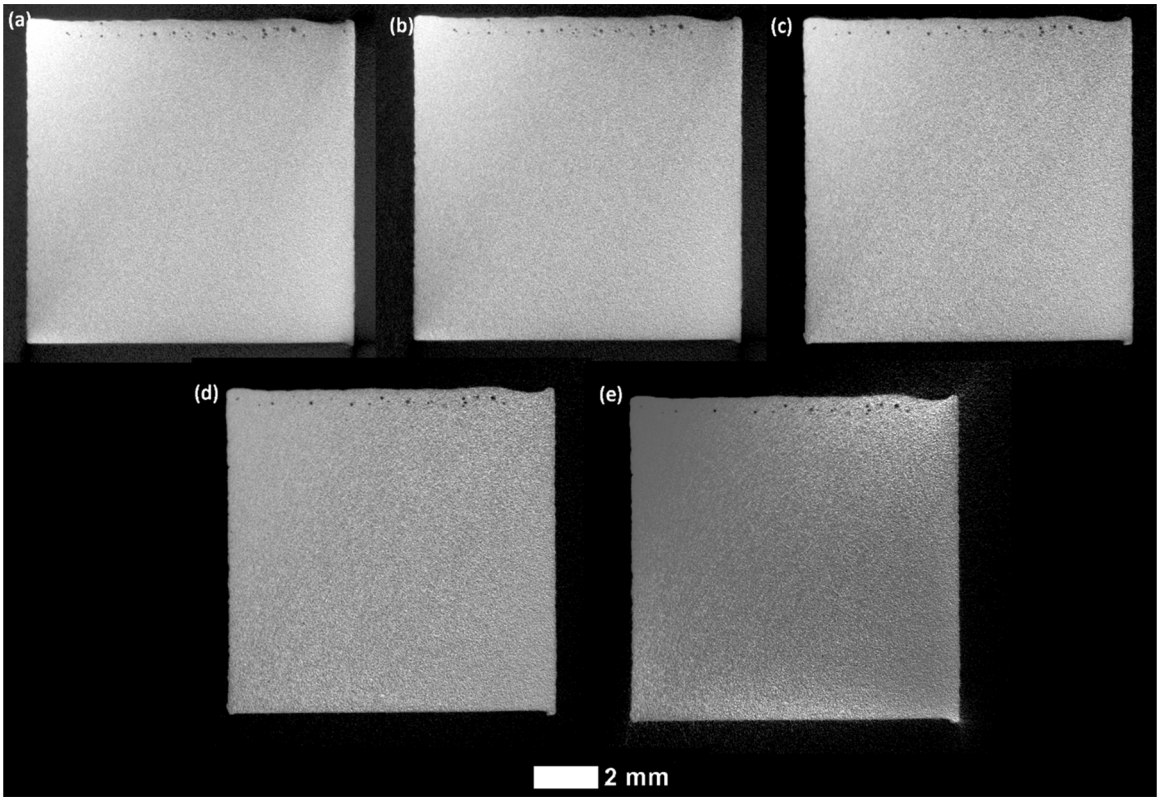

Fig. 12. Representative CT slice images for varying beam hardening correction factors of (a) 0; (b) 5; (c) 8; (d) 9.0 and (e) 9.5.

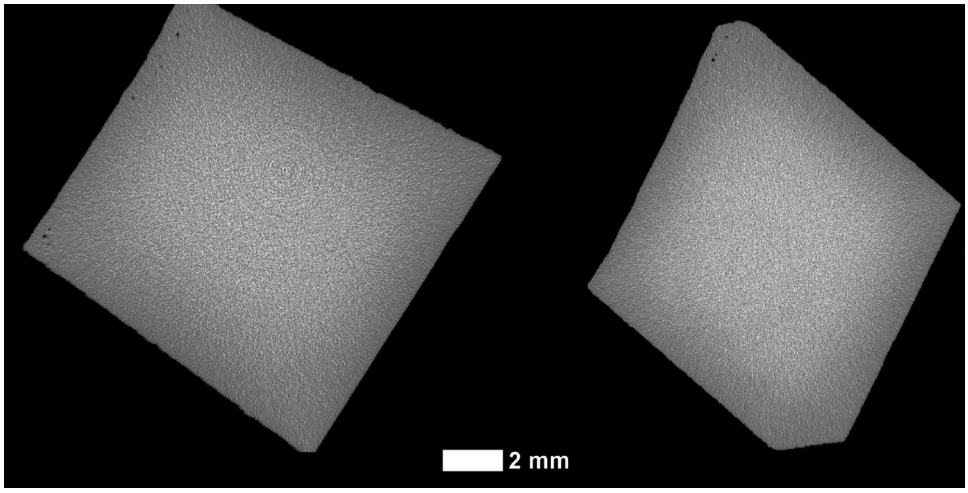

Fig. 14. Rotation ring artifact and detector-shift to remove rings – the image quality values are nearly identical.

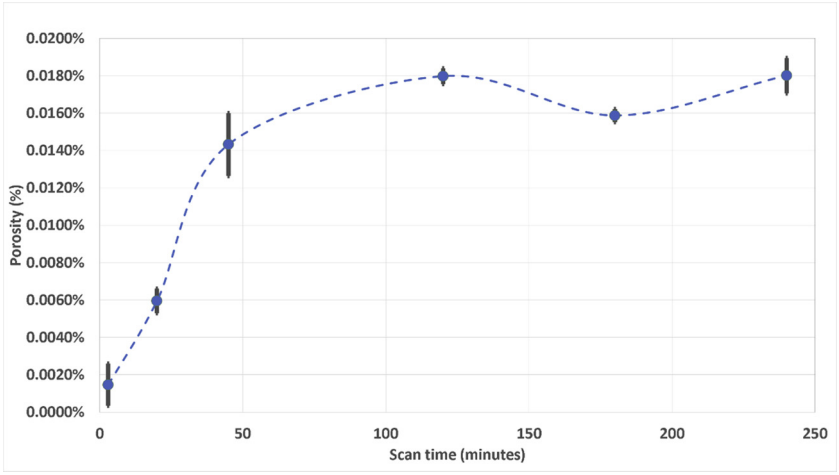

Fig. 15. Porosity quantification in cubes as a function of scan time, standard deviations are shown for 6 repeated measurements using the same workflow and analyst.

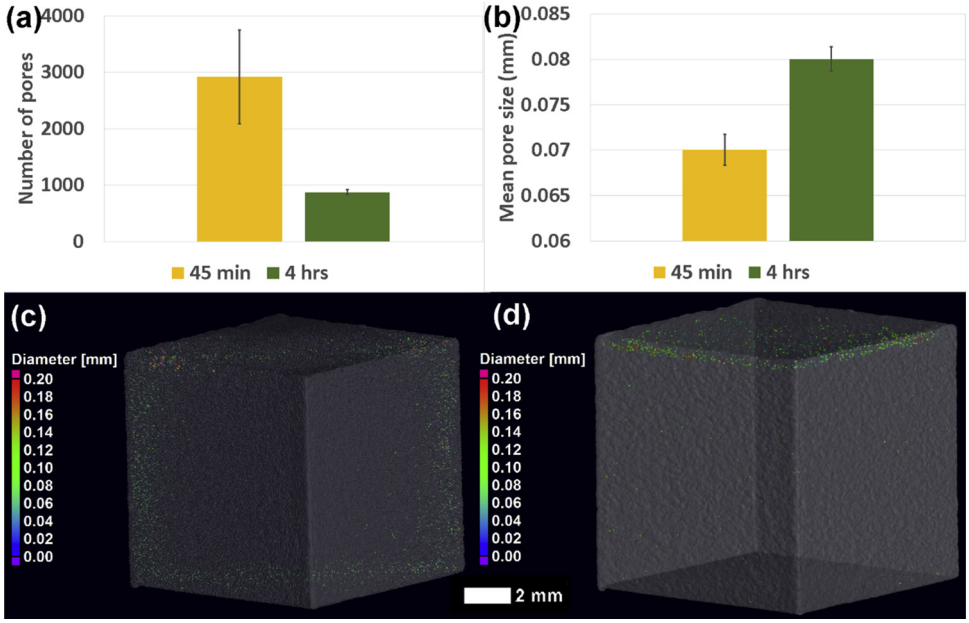

Fig. 16. Quantitative analysis of 3D porosity analysis results as a function of scan time shown here for 45 min vs 4 hs: (a) total number of detected pores and standard deviation over 5 repetitions, (b) mean pore size and standard deviation over 5 repetitions, (c) 3D result of 45 min, (d) 3D result of 4 hs.

due to the small pore sizes and small total porosity content. For example, the 2hr-scan has a slightly lower porosity value with narrow range of deviation. This can be attributed to system variations between this scan and the rest as this scan was done on a different day. The result is that its Q2 quality factor is similarly slightly lower than that of the 1 h and 3 h scans as shown in Fig. 3.

Quantitative comparison between scans at 45 min and at 4 h is seen in Fig. 16: the number of pores detected at 45 min is higher with a larger deviation between analyses. As mentioned above, pores are missed in this scan but the number of pores detected is higher as many false pores are detected which are close to the noise level (very small pores which are due to noise). For this reason the mean pore size of the 45 min scan is lower, due to the false pores detected. The 3D images demonstrate this difference between 45 min and 4 h scans, with the 4 h scan showing the expected porosity location at one surface only with spherical morphology. The quantitative analysis is reasonable for such small pores and the reproducibility and precision will likely increase for larger pores, or higher scan quality.

5. Conclusion

This work has demonstrated a simple image quality measurement method applicable to microCT. The quality measurements Q1 and Q2 are sensitive to most errors that can occur as demonstrated: Q1 is more sensitive to contrast and noise, while Q2 is more sensitive to image blur. The combination of quality factors is shown to be sensitive to all major image artifacts found in microCT scans and which can affect the ability to detect or quantify features of interest. The only exception is the centre-of-rotation rotation ring artifacts which are not very serious in the case reported and might be detected by these quality measures when occurring in a more excessive manner. This latter artifact has minimal influence on typical analyses and can be mitigated by either detector-shift during scanning, or by software elimination of pores in the location of the rotation axis. Additional artifacts may occur in various different systems which could not all be induced in this study, the most important of which is geometrical unsharpness or blur, due to the use of a large X-ray spot for too small voxel size. This results in a blur on the edge of the X-ray projection image which translates to the CT images. However this effect could not be induced with the nanoCT with the limited range of power of the X-ray tube available, and limited dynamic range of this detector. It is expected that this will negatively influence the Q2 value for increasing values of X-ray tube current.

For the special case of the 10 mm cube of Ti6Al4V, the porosity quantification was done according to the previously defined workflow. It was shown how an increase in scan time correlates with an improved analysis reproducibility and similar results for image quality values above $Q1 > 4$ and $Q2 > 3$. Despite the challenging nature of this quantitative analysis ($\sim$0.018 % porosity), the results clearly show the utility of using image quality metrics in combination with analysis results. The potential exists for defining minimum quality thresholds to improve the confidence in obtained results for any quantitative analysis by microCT and will even be valuable for qualitative inspection purposes. It is important to realize that the image quality measures reported here are for a homogenous material (e.g. a coupon sample) and these measures may be unsuited to multi-materials or materials with great density or compositional differences. It is hoped that these image quality metrics are used widely to support MicroCT-based materials analysis. By providing evidence of good image quality in CT images, analysis results can be trusted and improved usage of the technique can be ensured.

Acknowledgements

The Collaborative Program for Additive Manufacturing (CPAM), funded by the South African Department of Science and Innovation, is acknowledged for financial support.

Appendix A. Supplementary data

Supplementary material related to this article can be found, in the online version, at doi:https://doi.org/10.1016/j.mtcomm.2019.100792.

References

[1] E. Maire, P.J. Withers, Quantitative X-ray tomography, Int. Mater. Rev. 59 (2014) 1–43, https://doi.org/10.1179/1743280413Y.0000000023.
[2] V. Cnudde, M.N. Boone, High-resolution X-ray computed tomography in geosciences: a review of the current technology and applications, Earth-Science Rev. 123 (2013) 1–17, https://doi.org/10.1016/j.earscirev.2013.04.003.
[3] A. du Plessis, W.P. Boshoff, A review of X-ray computed tomography of concrete and asphalt construction materials, Constr. Build. Mater. 199 (2019) 637–651, https://doi.org/10.1016/j.conbuildmat.2018.12.049.
[4] A. du Plessis, I. Yadroitsev, I. Yadroitsava, S.G. Le Roux, X-ray microcomputed tomography in additive manufacturing: a review of the current technology and applications, 3D print, Addit. Manuf. 5 (2018), https://doi.org/10.1089/3dp.2018.0060 3dp.2018.0060.
[5] S.C. Garcea, Y. Wang, P.J. Withers, X-ray computed tomography of polymer composites, Compos. Sci. Technol. 156 (2018) 305–319, https://doi.org/10.1016/J.COMPSCITECH.2017.10.023.
[6] A. du Plessis, C. Broeckhoven, A. Guelpa, S.G. le Roux, Laboratory x-ray micro-computed tomography: a user guideline for biological samples, Gigascience 6 (2017) 42–49, https://doi.org/10.1093/gigascience/gix027.
[7] C. Broeckhoven, A. du Plessis, X-ray microtomography in herpetological research: a review, Amphibia-Reptilia. 39 (2018) 377–401.
[8] A. du Plessis, C. Broeckhoven, Looking deep into nature: a review of micro-computed tomography in biomimicry, Acta Biomater. 85 (2019) 27–40, https://doi.org/10.1016/j.actbio.2018.12.014.
[9] L. De Chiffre, S. Carmignato, J.-P. Kruth, R. Schmitt, A. Weckenmann, Industrial applications of computed tomography, CIRP Ann. 63 (2014) 655–677, https://doi.org/10.1016/J.CIRP.2014.05.011.
[10] A. du Plessis, S.G. le Roux, M. Tshibalanganda, Advancing X-ray micro computed tomography in Africa: going far, together, Sci. Afr. 3 (2019) e00061, , https://doi.org/10.1016/j.sciaf.2019.e00061.
[11] H. Villarraga-Gómez, E.L. Herazo, S.T. Smith, Progression of X-ray computed tomography from medical imaging to current status in dimensional metrology, Precis. Eng. (2019), https://doi.org/10.1016/J.PRECISIONENG.2019.06.007.
[12] H. Villarraga-Gómez, C. Lee, S.T. Smith, Dimensional metrology with X-ray CT: a comparison with CMM measurements on internal features and compliant structures, Precis. Eng. 51 (2018) 291–307, https://doi.org/10.1016/J.PRECISIONENG.2017.08.021.
[13] A. Townsend, R. Racasan, R. Leach, N. Senin, A. Thompson, A. Ramsey, D. Bate, P. Woolliams, S. Brown, L. Blunt, An interlaboratory comparison of X-ray computed tomography measurement for texture and dimensional characterisation of additively manufactured parts, Addit. Manuf. 23 (2018) 422–432, https://doi.org/10.1016/j.addma.2018.08.013.
[14] M. Ferrucci, R.K. Leach, C. Giusca, S. Carmignato, W. Dewulf, Towards geometrical calibration of x-ray computed tomography systems - a review, Meas. Sci. Technol. 26 (2015), https://doi.org/10.1088/0957-0233/26/9/092003.
[15] F. Léonard, S.B. Brown, P.J. Withers, P.M. Mummery, M.B. McCarthy, A new method of performance verification for x-ray computed tomography measurements, Meas. Sci. Technol. 25 (2014) 065401, , https://doi.org/10.1088/0957-0233/25/6/065401.
[16] Y. Liu, A.M. Kiss, D.H. Larsson, F. Yang, P. Pianetta, To get the most out of high resolution X-ray tomography: a review of the post-reconstruction analysis, Spectrochim. Acta Part B At. Spectrosc. 117 (2016) 29–41, https://doi.org/10.1016/J.SAB.2016.01.002.
[17] M. Tshibalanganda, A. Plessis, S.G. Le Roux, R.M.H. Smith, C. Browning, W.L. Taylor, Systematic experiments to quantitatively assess image quality for CT scans of a karoo tetrapod fossil, Palaeontol. Africana. (2019) 1–13.
[18] Y. ZHANG, P. MOSTAGHIMI, R.T. ARMSTRONG, On the challenges of grey-scale-based quantifications using X-ray computed microtomography, J. Microsc. 275 (2019) 82–96, https://doi.org/10.1111/jmi.12805.
[19] Q. Lin, M. Andrew, W. Thompson, M.J. Blunt, B. Bijeljic, Optimization of image quality and acquisition time for lab-based X-ray microtomography using an iterative reconstruction algorithm, Adv. Water Resour. 115 (2018) 112–124, https://doi.org/10.1016/j.advwatres.2018.03.007.
[20] P. Shan, X. Lai, Influence of CT scanning parameters on rock and soil images, J. Vis. Commun. Image Represent. 58 (2019) 642–650, https://doi.org/10.1016/j.jvcir.2018.12.014.
[21] R.L. Oakes, M.H. Chase, M.E. Siddall, J.A. Sessa, Testing the impact of two key scan parameters on the quality and repeatability of measurements from CT scan data, Palaeontol. Electron. Accepted (2019) (n.d.).
[22] ASTM E1695, Standard Test Method for Measurement of Computed Tomography (CT) System Performance, (1995), pp. 1–4 http://cdsweb.cern.ch/record/522402.
[23] F.A. Arenhart, V.C. Nardelli, G.D. Donatelli, Comparison of surface-based and image-based quality metrics for the analysis of dimensional computed tomography data, case stud, Nondestruct. Test. Eval. 6 (2016) 111–121, https://doi.org/10.1016/J.CSNDT.2016.05.002.
[24] M. Reiter, D. Weiß, C. Gusenbauer, M. Erler, C. Kuhn, J. Kastner, Evaluation of a

histogram-based image quality measure for X-ray computed tomography, ICT Conf. (2014) 273–282 www.3dct.at.
[25] W.A. Kalender, Computed Tomography: Fundamentals, System Technology, Image Quality, Applications, John Wiley & Sons, 2011 (Accessed January 19, 2016), https://books.google.com/books?hl=en&lr=&id=gfLWmRjoyPMC&pgis=1.
[26] A. Stolfi, L. De Chiffre, S. Kasperl, Error sources, Ind. X-Ray Comput. Tomogr. Springer International Publishing, Cham, 2018, pp. 143–184, https://doi.org/10.1007/978-3-319-59573-3_5.
[27] A.C. Kak, M. Slaney, Principles of computerized tomographic imaging (society for industrial and applied mathematics), Soc. Ind. Appl. Math. (2001), https://doi.org/10.1137/1.9780898719277 (Accessed January 19, 2016).
[28] A. du Plessis, S. le Roux, J. Waller, P. Sperling, E. Al, Laboratory X-ray tomography for metal additive manufacturing: round robin test, Addit. Manuf. Accepted (2019) (n.d.).
[29] A. du Plessis, P. Sperling, A. Beerlink, L. Tshabalala, S. Hoosain, N. Mathe, G. Stephan, MethodsX standard method for microCT-based additive manufacturing quality control 1 : porosity analysis, MethodsX 5 (2018) 1102–1110, https://doi.org/10.1016/j.mex.2018.09.005.
[30] A. du Plessis, S.G. le Roux, A. Guelpa, The CT scanner facility at Stellenbosch university: an open access X-ray computed tomography laboratory, Nucl. Instrum. Methods Phys. Res. Sect. B Beam Interact. Mater. Atoms. 384 (2016) 42–49, https://doi.org/10.1016/J.NIMB.2016.08.005.
[31] A. du Plessis, S.G. le Roux, Standardized X-ray tomography testing of additively manufactured parts: a round robin test, Addit. Manuf. 24 (2018) 125–136, https://doi.org/10.1016/j.addma.2018.09.014.
[32] T. Debroy, H.L. Wei, J.S. Zuback, T. Mukherjee, J.W. Elmer, J.O. Milewski, A.M. Beese, A. Wilson-Heid, A. De, W. Zhang, Additive manufacturing of metallic components – process, structure and properties, Prog. Mater. Sci. 92 (2018) 112–224, https://doi.org/10.1016/j.pmatsci.2017.10.001.